Theor Chem Acc (2005) 114: 318–326
DOI 10.1007/s00214-005-0680-x

REGULAR ARTICLE

Michal Straka · Martin Kaupp · Emil Roduner

Understanding solvent effects on hyperfine coupling constants of cyclohexadienyl radicals

Received: 31 May 2005 / Accepted: 13 June 2005 / Published online: 30 September 2005

Abstract Quantum chemical calculations have been carried out to understand better solvent effects on the isotropic muon and proton hyperfine coupling constants in the $C_6H_6Mu^\bullet$ radical. Both polarizable continuum solvent models and explicit inclusion of water molecules into supermolecular complexes were used. Changes in the hyperfine couplings of in-plane hydrogen atoms are very small and difficult to discuss, partly due to relatively large experimental error bars. In contrast, the out-of-plane proton and muon hyperfine couplings exhibit more pronounced changes. These are partly due to structural changes of the radical and partly due to direct electronic polarization effects. Polarizable continuum solvent models agree well with experimental changes for benzene but overshoot the enhancement of the hyperfine couplings for water. Explicit inclusion of water molecules reduces this overestimated spin density increase and thereby tends to bring theory and experiment into closer agreement. The enhancement of the spin density on the out-of-plane hydrogen or muon atoms by the solvent environment is mainly due to an increased polarization of the singly occupied MO towards this side.

Keywords Cyclohexadienyl radical · Density functional theory · Spin density · Hyperfine coupling · Solvent effects

Electronic Supplementary Material Supplementary material is available for this article at http:// dx.doi.org/10.1007/s00214-005-0680-x

M. Straka
Department of Chemistry,
P.O. Box 55 (A .I. Virtasen aukio 1) University of Helsinki,
FIN-00014, Helsinki, Finland.
Fax: +358-9-19150279

M. Straka · M. Kaupp (✉)
Institut für Anorganische Chemie,
Am Hubland, 97074 Würzburg,
Germany
E-mail: kaupp@mail.uni-wuerzburg.de

E. Roduner
Institut für Physikalische Chemie,
Universität Stuttgart, Pfaffenwaldring 55, 70569, Stuttgart,
Germany
E-mail: e.roduner@ipc.uni-stuttgart.de

1 Introduction

The electron spin resonance spectrum of the cyclohexadienyl radical, $C_6H_7^\bullet$, has been of interest since its discovery more than four decades ago [1, 2]. In recent years, the emphasis has been on its use as a spin label for the investigation of as diverse environments as lipid membranes or zeolite cages, either by EPR on cyclohexadienyl itself [3], or by muon spin resonance (μSR) on the muoniated cyclohexadienyl analogue, $C_6H_6Mu^\bullet$ [4]. However, in contrast to the more widely used nitroxide spin labels, the effect of environment on the EPR parameters of cyclohexadienyl is much less understood. In the case of nitroxides, the $g-$tensor component along the N-O bond direction (g_{xx}) and the nitrogen hyperfine coupling component perpendicular to the plane of the ring structure (A_{zz}) have been applied to probe solvent polarity and hydrogen bonding of the local environment. The dependence of these parameters on the dielectric constant was investigated both experimentally and using theoretical methods and is reasonably well understood [5]. These effects served also to determine, e.g., the degree of water penetration into the hydrophobic region of phosholipid membranes [5–7], the polarity and hydrogen bonding ability at various spin-label sites of the protein bacteriorhodopsin [8] or the location of water uptake into cotton [9]. It is mainly the detailed understanding of environmental effects on their EPR parameters that makes these spin labels so valuable.

In the context of the use of $C_6H_6Mu^\bullet$ as a spin probe in zeolites, [4] the effect of a sodium cation on its hyperfine parameters has been modelled theoretically [10]. More recently, $C_6H_6Mu^\bullet$ has been used to study the partitioning of co-surfactant molecules between the polar aqueous and the non-polar lipid environments of lamellar phase surfactant dispersions [3]. These types of measurements provide evidence of a gradient of water molecules from the water – surfactant interface into the bulk of the surfactant structure. However, the *ortho*-, *meta*-, and *para*-isomers of the substituted cyclohexadienyl radicals revealed partly conflicting polarity information, even in isotropic solutions. This

illustrates the need for a better understanding of the solvent effects in cyclohexadienyl-based radicals.

Compared to the relatively localized nitroxides, cyclohexadienyl-type radicals are more delocalized species with a relatively rigid ring. Furthermore, the hydrogen bonding ability of the delocalized π-system is expected to be quite different from that of the N–O group. It is the aim of the present work to discern the mechanism of the solvent effects and to distinguish between its geometrical and electronic origins. In view of this, experimental hyperfine coupling constants (HFCs) from μSR experiments on $C_6H_6Mu^\bullet$ in the gas phase, in liquid benzene, and in liquid water are compared with calculated values based on hybrid density functional methods of radicals complexed with water molecules and/or embedded in a polarizable dielectric continuum.

2 Methods section

The $C_6H_7^\bullet$ radical model. Muonium (Mu$\equiv \mu^+e^-$) can be regarded as a light isotope of hydrogen [11]. When considering isotope effects on HFCs, the muon differs from the proton in two aspects. The ratio of their magnetic moments, $\mu_\mu/\mu_p = 3.1833$, makes the muon–electron hyperfine coupling for a given radical structure larger by this factor as compared to the proton. The coupling is further increased by about 20% by the so-called *intrinsic isotope effect* [12], originating from the anharmonicity of the C–Mu(C–H) potential energy curve which renders the C–Mu bond approximately 5% longer than the C–H bond on a vibrational average [12]. As an indirect consequence, the remaining methylene C–H bond is shortened on an average, and the coupling of the proton decreases by about 6%.

Limited by the available computational resources we model the $C_6H_6Mu^\bullet$ radical by $C_6H_7^\bullet$. This corresponds to a static picture in which the calculated structures of both radicals are identical and the muon HFC can be obtained by calculating the proton HFC in $C_6H_7^\bullet$ and multiplying it by the ratio of muon and proton magnetic moments $\mu_\mu/\mu_p = 3.1833$. The intrinsic isotope effect and the influence of internal and external dynamics on hyperfine couplings are thus neglected completely in our calculations. We assume that the solvent effects on $C_6H_7^\bullet$ will not differ much from those of $C_6H_6Mu^\bullet$, and that the influence of ro-vibrational effects will cancel largely in comparisons of solvated and gas-phase radicals.

Calculation of hyperfine coupling constants. The hyperfine coupling tensor A^N corresponds to the interaction of the magnetic moments of unpaired electrons with nucleus N. Up to first-order perturbation theory, there are two contributions to hyperfine coupling constants in light-atom systems [13] (neglecting second-order spin-orbit corrections):

$$A^N = A^N_{FC} + A^N_{SD} \tag{1}$$

Here A_{FC} and A_{SD} correspond to the Fermi-contact and spin-dipolar terms. In the gas phase or in liquid isotropic solution, A^N_{SD} averages to zero due to fast tumbling, and only A^N_{FC} will contribute. A^N_{FC} is related to the spin density $\delta(\mathbf{r}_N)$ at nucleus N via

$$A^N_{FC} = -\frac{2}{3} g_e \gamma_e \gamma_N \mu_0 \delta(r_N), \tag{2}$$

where g_e is the g-value of the free electron (2.002319), γ_e and γ_N are electronic and nuclear magnetogyric ratios, respectively, and μ_0 is the vacuum permeability. In particular,

$$A_p = -\frac{2}{3} g_e \gamma_e \gamma_p \mu_0 \delta(r_p) \tag{3a}$$

$$A_\mu = -\frac{2}{3} g_e \gamma_e \gamma_\mu \mu_0 \delta(r_\mu) \tag{3b}$$

If $\delta(r_p) = \delta(r_\mu)$, as is the case in our model, division of (3b) by (3a) gives

$$\frac{A_\mu}{A_p} = \frac{\gamma_\mu}{\gamma_p} = \frac{\mu_\mu}{\mu_p} \tag{4}$$

This relation will be used for comparison of experimental and calculated A_μ.

Modelling solvation effects. The solvation effects may be divided into contributions from long-range isotropic dielectric effects and from specific hydrogen bonding. The former can be computationally described by polarizable continuum models (PCM), in which the solvent is considered as a uniform polarizable medium with dielectric constant ε, forming a cavity around the solute. Hydrogen-bonding effects are best taken into account by including explicit solvent molecules in computations on supermolecular model complexes. For nonpolar solvents such as benzene we expect negligible hydrogen bonding. The conductor-like polarizable continuum model (CPCM) [14–18] used in this work is expected to give reasonable results. In aqueous solution, hydrogen bonding to the delocalized π-system of the radical and with the methylene site may be important and will be studied by supermolecular models with two or four explicit water molecules, either instead of or in addition to the continuum solvent model.

Computational details. Most calculations were done at B3LYP hybrid density functional level [19–21], using the Gaussian 03 program package [22]. Convergence criteria *scf = tight* (energy and density matrix convergence 10^{-8} Å) and integration grid option *grid=ultrafine* (99 radial shells and 590 angular points per shell) were used to ensure good numerical accuracy. The 6-311+ G(d,p) [23,24] basis set was used for structure optimization, and EPR-III [25] basis for hyperfine calculations. The B3LYP/EPR-III level is known to provide accurate hyperfine coupling constants for organic radicals [26]. The CPCM [14–18] model as implemented in Gaussian 98 was used to include dielectric continuum solvent effects. Natural population analyses (NPA) [27,28] were employed to calculate atomic charges. Molecular structures, orbitals, and spin-density isosurfaces are displayed with the Molekel 4.0 program [29,30].

Table 1 Experimental and calculated isotropic hyperfine couplings in MHz for $C_6H_6Mu^\bullet$ and $C_6H_7^\bullet$ radicals[a]

Solvent	Experiment			Calculations						
	Gas-phase[b]	Liquid benzene[c]	Liquid water[e]	Gas -phase	CPCM (benzene)	CPCM (water)	Gas-phase +2 H_2O	Gas -phase +4 H_2O	CPCM (water) +2 H_2O	CPCM (water) +4 H_2O
A_μ Mu_{ipso}	507.5(6)	513.24(1)[c] (+1.1%)	518.54(15) (+2.2%)							
$A_\mu \times \mu_\mu/\mu_p$ Mu_{ipso}	159.4(2)	161.23(3)[c] (+1.1%)	162.89(5) (+2.2%)	149.2	150.6 (+0.9%)	155.7 (+4.3%)	150.3 (+0.7%)	157.9 (+5.8%)	155.2 (+4.0%)	150.6 (+0.9%)
A_p H_{ipso}	124.9(6)	125.89(2)[c] (0.8%)	127.14(5) (+1.8%)	149.2	150.6 (+0.9%)	155.7 (+4.3%)	150.3 (+0.7%)	157.9 (+5.8%)	155.2 (+4.0%)	150.6 (+0.9%)
A_p H_{ortho}	−24.8(7)	−25.14(4)[d] (+1.4%)	−25.47(7) (+2.7%)	−27.8	−27.7 (−0.4%)	−27.5 (−1.0%)	−27.4 (−1.4%)	−26.8 (−3.7%)	−27.0 (−2.9%)	−27.2 (−2.2%)
A_p H_{meta}	8.2(9)	7.47(4)[d] (−8%)	–	9.9	9.8 (−1.0%)	9.6	9.5	9.1	9.0	9.4
A_p H_{para}	−36.4(9)	−36.19(4)[d] (−0.5%)	−36.43(7) (0.0%)	−37.3	−37.2 (−0.3%)	−37.1 (−0.5%)	−37.5 (+0.5%)	−37.4 (+0.2%)	−37.5 (+0.5%)	−37.9 (+1.6%)

[a] Experimental values at 40°C. Calculations at B3LYP/EPR-III level. Percentage increase relative to gas-phase value in parentheses for both experiment and computation. Isotropic values for $C_6H_7^\bullet$ in 1M NaOH (at pH=14) are 134.6, −25.2, 7.5, −36.8 MHz for ipso-, ortho-, meta-, and para- protons, respectively (Eiben K, Schuler RH (1975), J Chem Phys 62:3093).

[b] Ref. [43] Fleming DG, Arsenau DJ, Pan JJ, Shelley MY, Senba M, Percival PW (1997) Appl Magn Reson 13:181.

[c] Ref. [44] Yu D, Percival PW, Brodovitch JC, Leung SK, Kiefl RF, Venkateswaran K, Cox SFJ (1990) Chem Phys 142:229.

[d] Ref. [45] Percival PW, Kiefl RF, Kreitzman SR, Garner DM, Cox SFJ, Luke GM, Brewer JH, Nishiyama K, Venkateswaran K (1987) Chem Phys Lett 133:465. (measured at 27°C and extrapolated to 40°C).

[e] Measured relative to liquid benzene, experimental details to be published.

3 Results and discussion

3.1 Optimized structures

Figure 1 shows B3LYP/6-311+ G(d,p) optimized structures of various models. Optimization of $C_6H_7^\bullet$ in the gas phase, as well as in benzene and water solutions at CPCM level (without explicit solvent molecules) provided the expected C_{2v} structure (Fig. 1a–c), with planar carbon skeleton, in-plane *ortho*-, *meta*-, and *para*-hydrogens, as well as two out-of-plane methylene hydrogens, H_{ipso}. The structure changes due to CPCM solvent effects are not large but notable, especially with water. The largest changes are observed for the out-of-plane C–H(Mu) distance, which contracts by 0.002 Å in benzene and expands by 0.004 Å in water, compared to the computed gas-phase value of 1.105 Å. The out-of plane bond angle of about 103° does not appear to be sensitive to solvation at the CPCM level.

Two explicit water molecules, added to the gas-phase model, will bond to the π-system by weak T-stacked hydrogen contacts above the center of the shortest C–C bond (C_{ortho}–C_{meta}), with the oxygen slightly displaced towards the ring center (Fig. 1d). Experimental, quantum chemical, and molecular dynamics simulation studies of the related benzene–water complex point to a structure with hydrogen bonded direct to the ring center, and the water oxygen pointing away from the benzene plane [31–36]. Simulations and experiments show that in the benzene complex, water can rearrange via structures with both water hydrogens pointing towards the π-system [31–36]. In the present $C_6H_7^\bullet$ $(H_2O)_2$ model, the shortest (HO)H. . .C distances are 2.554 and 2.617 Å. The C–H(Mu) distance is slightly shortened compared to the free radical. Bringing this model into the CPCM cavity (Fig. 1f) leads to more asymmetric (HO)H. . .C distances of 2.387 and 2.668 Å and to an elongation of the C-H(Mu) distance as compared to the CPCM calculation without explicit water molecules (Fig. 1c). This shows that the effects of the continuum solvent model and of explicit water molecules on the structure of the radical are not additive, and that the structure of the supermolecular complex is influenced non-negligibly by the further environment. Attempts to locate an isomer with water molecules bonded to $H(Mu)_{ipso}$ via oxygen converged always to the structure shown in Fig. 1d. In the benzene–water complex, an isomer in which water is bonded via oxygen to a hydrogen was calculated to lie higher in energy (5 kJ/mol) than the structure with an H-bond to the ring center [34]. The binding energy estimated here for the first two water molecules, $C_6H_7^\bullet + 2\ H_2O \rightarrow C_6H_7^\bullet \cdot\ 2H_2O$, is 18.0 kJ mol^{-1} at DFT level. Counterpoise-corrected MP2 energy calculations at DFT structures give 25.0 kJ mol^{-1}. This may be compared to experimental and theoretical binding energies of the benzene–water complex between ca. 6 and ca. 15 kJ mol^{-1} [31–36]. The difference between the hydrogen bond directed to the ring center in the benzene–water complex (not shown) and the cyclohexadienyl radical–water complexes with a preference for more "localized" H–bonding patterns towards the shortest C=C bonds (Fig. 1) appear to be notable.

Addition of four water molecules to the gas-phase radical (Fig. 1e) leads to a structure with close contacts of 2.40 Å from two water oxygen atoms to the out-of-plane proton (muon). Upon immersing this model into the CPCM cavity, the two extra water molecules move away from the out-of-plane positions, and no notable interaction remains

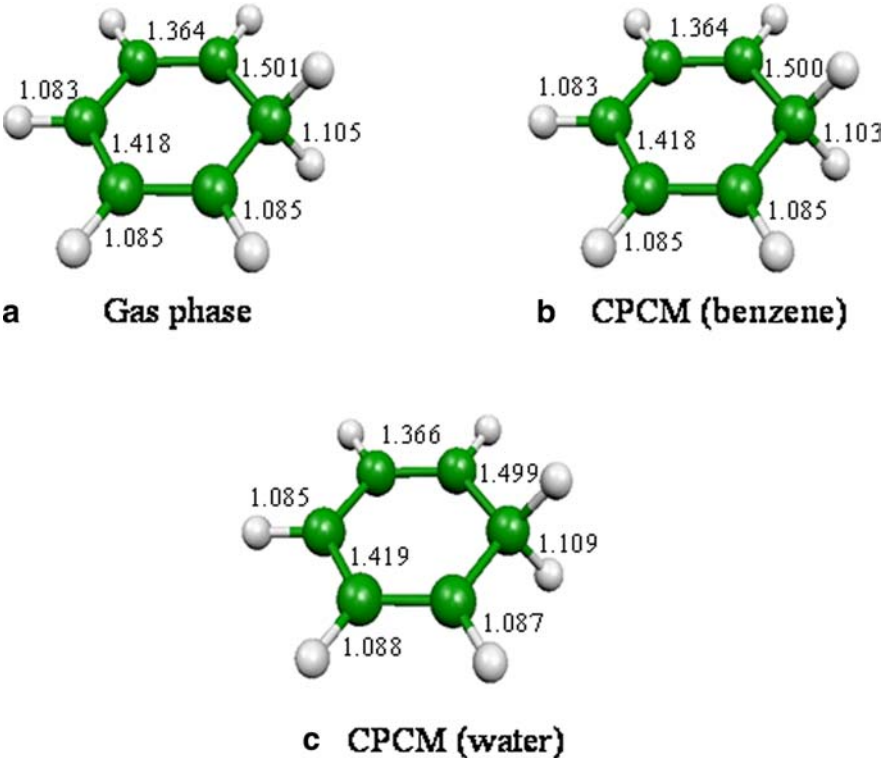

(a)

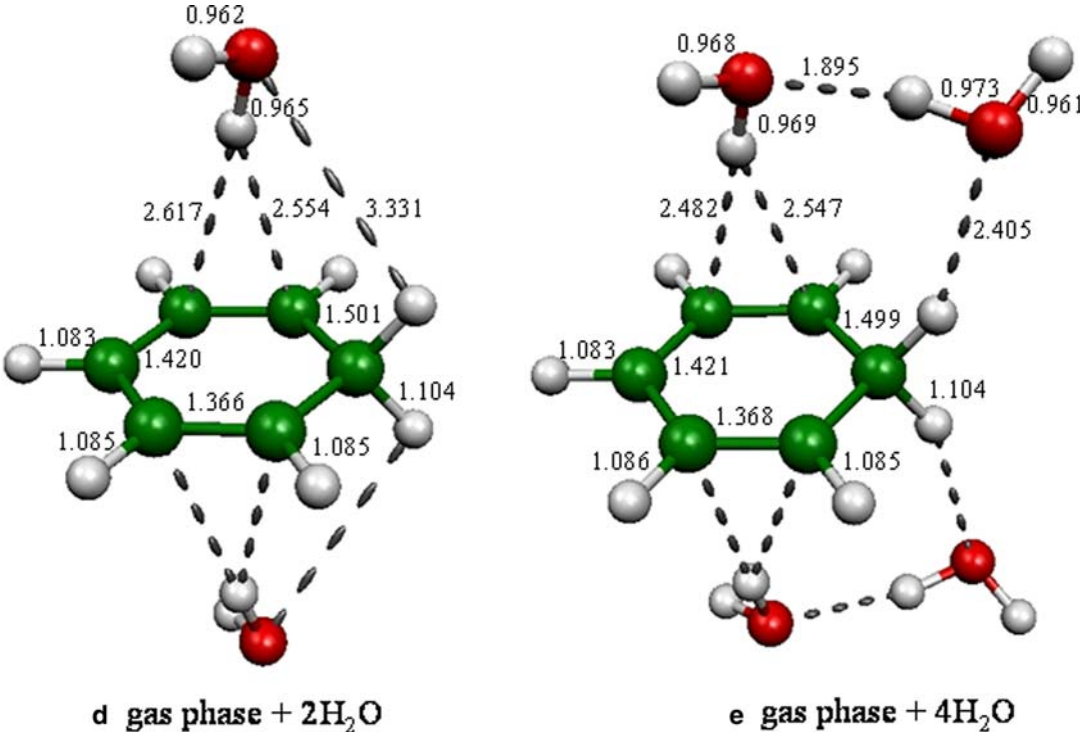

(b)

Fig. 1 Optimized structures of $C_6H_7^{\bullet}$ in the gas phase and using different solvation models at the B3LYP/6-311+G(d,p) level. Bond lengths in Å

(Fig. 1g). The C_{ipso}-H(Mu) distance shortens to 1.105 Å, which coincides with the gas-phase value. That is, the hydrogen bonding appears to counteract the structural effect of the continuum solvent model, and the continuum solvent in turn weakens explicit interactions between the CH_2-moiety and the nearest solvent molecules. These non-additive effects are relevant with respect to the solvent effects on HFCs (see following paragraph). In general, it appears that the interactions with explicit water solvent molecules are relatively weak. This makes the theoretical description of the situation in aqueous solution challenging, as large-amplitude motions within the first solvent shell are probable.

We note in passing, that modelling of sodium cation binding to cyclohexadienyl gave a complex in which the cation was above the ring, displaced somewhat towards C_{para} [10]. Effects on the intramolecular structure parameters included the shortening of the C-H_{ipso} bond on the same side as the cation by 0.004 Å, and a lengthening on the opposite side by 0.001 Å.

3.2 Comparison of computed and experimental hyperfine couplings

The antisymmetric linear combination of the two C_{ipso}-H σ-orbitals exhibits π-symmetry with respect to the molecular plane and delocalizes into the π-system by hyperconjugation [37,38]. This explains the relatively large hyperfine couplings of the methylene protons, H_{ipso}. Table 1 summarizes experimental and computed results for muon and proton isotropic hyperfine couplings (A_μ and A_p) in $C_6H_6Mu^\bullet$ and $C_6H_7^\bullet$ [39]. For easier comparison, the measured A_μ values were divided by the factor 3.1833 so that we can compare with computed proton values. Our computed gas-phase values are in reasonable agreement with previous DFT calculations [10,38], and agree better with the experimental values for the H_{ipso} positions than previous CIS [10,40] and coupled-cluster studies [41] (in the latter case probably the too small DZP basis sets limited the accuracy larger basis sets are needed to reproduce hydrogen HFCs in coupled-cluster calculations [42,43]). Notably, the computed static A_p (H_{ipso}) values for $C_6H_7^\bullet$ are higher than experiment for the H_{ipso} position in $C_6H_6Mu^\bullet$ but somewhat lower than the scaled A_μ value. This reflects our neglect of ro-vibrational effects (see earlier para). In view of this, and of the inherent dependence of the results on exchange-correlation functional (Table S1 in Supporting Information), the uncertainties of the computed HFCs are clearly larger than the solvent effects we want to study. We assume, however, that these systematic errors cancel out mostly when looking at the differences between gas phase and different solvent environments.

Solvent effects for the in-plane protons are very small. Due to the relatively large experimental error bars in the gas phase, it becomes impossible to discuss the solvent effects on the HFCs for these positions in more detail. Even if more accurate experimental data were available, more refined computations would be needed for a reliable discussion, including dynamical solvent effects and a more realistic treatment of hydrogen bonding. We will thus in the following concentrate on the proton and muon HFCs for the methylene (H_{ipso}) positions, with the aim to understand solvent effects on these.

Computed solvation effects for A_p (H_{ipso}) agree reasonably well with the experimental trends. At CPCM level, A_p (H_{ipso}) increases from the gas phase through benzene to aqueous solution, but the trend appears to be overestimated by the CPCM calculations. Inclusion of two explicit water molecules into the CPCM(water) cavity improves the trend by a slight decrease of A_p (H_{ipso}). Inclusion of another two explicit water molecules decreases the coupling constant further, but

Table 2 Computed hyperfine couplings (in MHz) in $C_6H_7^\bullet$ at different levels of including solvent effects[a]

Solvent	Gas-phase// gas-phase	CPCM(water)// gas-phase	CPCM(water)// CPCM(water)	Gas-phase// CPCM(water)
A_p (H_{ipso})	149.2	152.9	155.7	152.0
A_p (H_{ortho})	−27.8	−27.5	−27.5	−27.8
A_p (H_{meta})	9.9	9.6	9.6	9.9
A_p (H_{para})	−37.3	−37.2	−37.1	−37.2

[a]CPCM results at B3LYP/EPR-III level. The notation of levels of including solvent effects is HFC-calculation//structure-optimization.

Table 3 Calculated orbital contributions[a] to A_p(ipso) in MHz

Orbital	Orbital symmetry	Gas-phase// gas-phase	CPCM (benzene)// CPCM (benzene)	CPCM (water)// CPCM (water)[b]	CPCM (water)// gas-phase
7	a_1	0.05	0.08	0.17 (1.8%)	0.14
8	b_2	0.00	0.00	0.00	0.00
9	a_1	−5.83	−5.70	−5.12 (+10.9%)	−5.39
10	a_1	19.70	19.68	19.17 (−8.2%)	19.31
11	b_2	0.00	0.00	0.00	0.00
12	a_1	−3.58	−3.51	−3.27 (+4.8%)	−3.43
13	a_1	12.30	12.31	12.58 (+4.3%)	12.09
14	b_2	0.00	0.00	0.00	0.00
15	b_1	−8.16	−8.24	−7.94 (+3.4%)	−7.49
16	b_2	0.00	0.00	0.00	−0.01
17	a_1	−4.21	−4.17	−3.96 (+3.8%)	−4.62
18	a_1	−0.28	−0.36	−0.82 (-8.3%)	−1.48
19	b_1	14.00	13.90	13.94 (−0.9%)	14.71
20	b_2	0.00	0.00	0.00	0.00
21	a_2	0.00	0.00	0.00	0.00
22 (SOMO)	b_1	125.30	126.61	131.03 (+4.6%)	129.06
$\sum$		149.29	150.60	155.78 (4.4%)	152.91

[a]Orbitals 1–6 do not contribute. See Fig. S1 (in Supporting Information) for orbital isosurface plots. [b]Percentage changes relative to the gas phase calculation shown in parentheses.

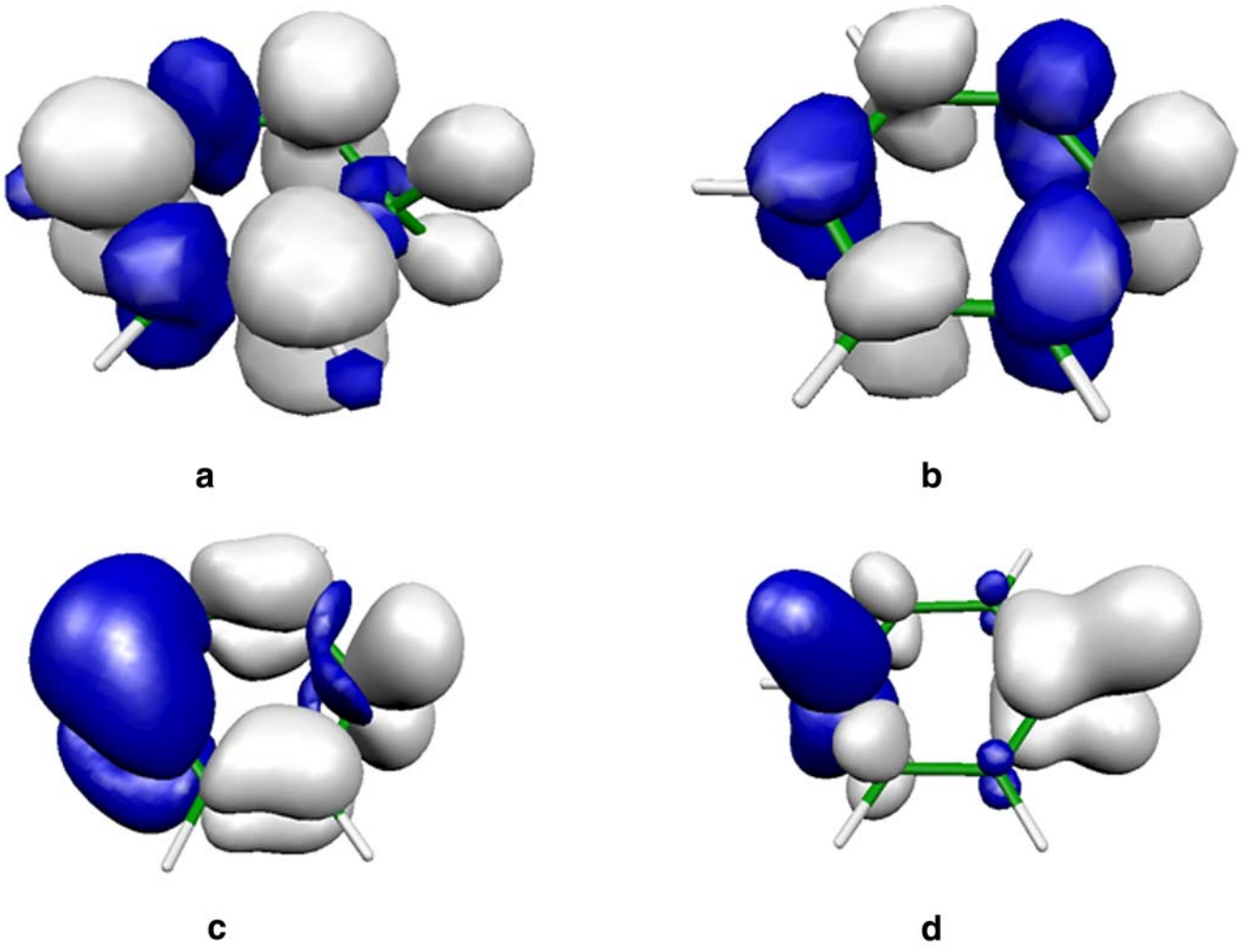

Fig. 2 Isosurface plots of computed gas-phase spin densities of $C_6H_7^\bullet$, and difference densities due to direct electronic continuum solvation effect. **a**) total gas-phase spin density (isosurface $\pm 10^{-3}$ a.u.), **b**) difference spin density for CPCM(water)//gas-phase minus gas-phase//gas-phase calculations (isosurface $\pm 10^{-4}$ a.u.), **c**) gas-phase SOMO spin density (isosurface $\pm 10^{-4}$ a.u.), **d**) difference SOMO spin density for CPCM(water)//gas-phase minus gas-phase//gas-phase calculations (isosurface $\pm 10^{-5}$Å)

now the overall solvation effect appears underestimated (Table 1). Notably, the opposite direction of the effects of continuum solvent and hydrogen bonding for $C_6H_7^\bullet(H_2O)_4$ has to do with the change of the hydrogen-bond geometry in the cavity of the CPCM model (Fig. 1). In particular, the short contacts between ipso proton (muon) and water oxygen atoms in the supermolecular model $C_6H_7^\bullet(H_2O)_4$ (Fig. 1e) do not persist in the presence of the continuum solvent (Fig. 1g). Interestingly, the HFC for the supermolecular complex is high. That is, hydrogen bonding and continuum solvent taken separately would both increase the hyperfine coupling substantially, but in combination the overall effect is much smaller. In view of the relatively complex behavior of hydrogen bonding, with a presumably rather shallow potential energy surface for rearrangement of the first solvent shell, molecular dynamics simulations at a relatively high computational level (suitable for describing the intermolecular interactions quantitatively) will be needed to obtain more accurate results.

Table 4 Computed dipole moments for $C_6H_7^\bullet$ in Debye[a]

Model	Dipole moment (Debye)
Gas-phase//gas-phase	0.54
CPCM(benzene)//CPCM(benzene)	0.66
CPCM(water)//CPCM(water)	0.97
CPCM(water)//gas-phase	0.96
Gas-phase//CPCM(water)	0.54

[a] At B3LYP/EPR-III level.

3.3 Further analysis of solvent effects on HFCs

Influence of intramolecular structural changes. We noticed that the structure of the radical is influenced by solvent effects (discussed earlier). In particular the C-H(Mu) bond lengths seem to be sensitive to solvation. How much is this reflected in the HFCs? While we cannot completely separate structural and electronic effects, we may estimate

Table 5 Computed NPA charges for $C_6H_7^{\bullet}$ at various levels of modelling solvation[a]

Atom	Solvent model				
	Gas-phase// gas phase	CPCM(benzene)// CPCM(benzene)	CPCM(water)// CPCM(water)	CPCM(water) + $2H_2O$// CPCM(water) + $2H_2O$	CPCM(water) + $4H_2O$// CPCM(water) + $4H_2O$
C_{ipso}	−0.52	−0.53	−0.55	−0.55	−0.55
H_{ipso}	0.24	0.24	0.26	0.27	0.26
C_{ortho}	−0.16	−0.16	−0.16	−0.19	−0.17
C_{meta}	−0.25	−0.26	−0.27	−0.27	−0.28
C_{para}	−0.22	−0.23	−0.24	−0.24	−0.23
H_{ortho}	0.21	0.21	0.22	0.23	0.23
H_{meta}	0.22	0.23	0.23	0.24	0.24
H_{para}	0.22	0.22	0.23	0.24	0.24

[a] At B3LYP/EPR-III level.

structural effects by performing a gas-phase HFC calculation at a solution-optimized structure or vice versa. Table 2 shows both gas-phase//CPCM(water) and CPCM(water)//gas-phase results. In the former calculation, $A_p(H_{ipso})$ is increased approximately by one-half of the total continuum solvent effect. Similarly, the latter calculation bridges about half of the total change. At this continuum solvent level, structural and direct electronic effects are thus of similar magnitude for $A_p(H_{ipso})$. We recall, however, that the CPCM model exaggerates the increase in $A_p(H_{ipso})$. The total solvent effect is actually only about 3.5 MHz experimentally, and the balance between structural and electronic effects may be shifted somewhat in more realistic treatments. We do not observe any direct relation between C–H(Mu) bond lengths and $A_p(H_{ipso})$. For the *ortho-*, *meta-*, and *para-* protons, the solvent effects on the computed HFCs appear to derive almost exclusively from the direct electronic contributions, with very little structural influences (but keep in mind that computed changes are small and do not follow the experimental trends well in these cases).

Spin density plots. The isotropic Fermi-contact HFC is directly proportional to the spin-density at the nucleus in question (Eqs. 2–3). Analyses of spin density are thus of interest, and spin-density isosurface plots might be further revealing. The computed spin-density surface for the gas-phase radical (Fig. 2a) reflects closely the computed isotropic couplings in Table 1. We observe positive spin densities (light grey) for H_{ipso}, and negative spin densities (dark grey) for H_{ortho} and H_{para}. The spin density at H_{meta} is very small and only visible at lower isosurface values. These results follow closely the previous analyses for the free radical by Adamo et al. [38].

The relatively small differences between gas-phase and various solvent calculations are not easily visualized directly by such plots. More information may be obtained from differences of spin densities, but these are restricted to comparison between calculations for one given structure. Figure 2b subtracts total spin densities of gas-phase//gas-phase calculations from CPCM(water)//gas-phase results. Obviously, the direct electronic effect of the continuum solvent model is mainly to increase the spin density at H_{ipso} and C_{ipso}, as well as at C_{meta}, and to decrease it at C_{ortho} and C_{para}. This explains the enhancement of $A_p(H_{ipso})$. Changes in the isotropic couplings of the in-plane hydrogens have to be transmitted by spin polarization through the associated C–H bonds and are therefore relatively small (larger changes will result for the dipolar couplings, but these are not observed in the available experiments).

Orbital analyses of spin density. Individual orbital contributions to the hyperfine couplings are provided in Table 3, and the orbitals are visualized in Fig. S1 in Supporting Information. The HFCs at H_{ipso} (and thus Mu_{ipso}) are dominated by a large positive contribution from the SOMO (orbital 22, it gives 125.3 MHz – 84% – in the gas-phase calculation), with additional positive contributions from orbitals 10, 13, and 19 (+19.7, +12.3, and +14.0 MHz, respectively). However, the solvent effect in the CPCM calculations derives almost exclusively from the enhancement of the SOMO contribution, whereas small changes in the spin-polarization contributions cancel largely (Table 3). Figure 2c shows the SOMO spin density (gas-phase) and Fig. 2d the difference spin density for the SOMO, obtained when subtracting the gas-phase//gas-phase spin density from the CPCM(water)//gas-phase result. The appreciable enhancement of SOMO spin density at H_{ipso} and C_{ipso} and the almost equally large negative contribution at C_{para} are clearly visible. Apparently, at least within the CPCM framework, the direct electronic solvation effect on the H_{ipso} or muon couplings derives not that much from spin polarization, but rather from a change in the direct SOMO contribution.

Dipole moments and NPA charges. In view of these results, we may ask in more detail in which way the interaction with the solvent affects the electronic structure of the radical, and in particular the composition of the SOMO. Notably, the computed dipole moments in Table 4 increase from 0.54 Debye in the gas phase to 0.95 Debye in the CPCM(water)//CPCM (water) calculations. Interestingly, the structural solvation effects on the dipole moment are negligible, and it is the direct mutual electronic polarization between solute and solvent that enhances the dipole moment. The increase of dipole moment is consistent with a larger charge separation in solution,

as confirmed by the NPA charges in Table 5. The increased positive charge on H_{ipso} and the enhanced negative charge on C_{ipso}, C_{meta}, and C_{para} are notable. Thus, the dielectric continuum solvent effects in water increase the dipole moment by an appreciable factor of almost two. Direct hydrogen bonding appears to partly compensate the continuum solvent effect on the HFCs of CPCM(water). A determination of an "isolated radical" dipole moment from the supermolecular calculations with explicit water molecules was unfortunately not possible. The NPA charges for the supermolecular complex with two water molecules (Fig. 1d) suggest a further enhancement of the positive charge on H_{ipso} (Table 5). Addition of two further water molecules (Fig. 1e) decreases the charge on H_{ipso}. While the calculated changes in the charges are small, their relation to the spin density suggests that both structural and electronic effects of hydrogen bonding influence electronic structure and thus spin density of $H(Mu)_{ipso}$. Apparently, the increased dipole moment induced by solvation is related indirectly to an enhanced "electron hole character" near H_{ipso}.

4 Conclusions

Solvent effects on the electronic structure, spin density, and hyperfine couplings of the cyclohexadienyl radical are far more subtle than on the more polar nitroxide spin labels, and they are thus more difficult to analyze. Changes in spin densities and HFCs at the in-plane hydrogen positions are too small, and the experimental error bars are too large to discuss solvent-effects on those couplings meaningfully in greater detail. In contrast, changes in the out-of-plane methylene hydrogen (or muon) positions are more notable and derive roughly to similar amounts from solvent-induced structure changes (mainly by a change of the C_{ipso}–H bond length) and from a direct electronic polarization of the spin density within the radical by the solvent at a given structure. While the modest increase of the out-of-plane HFCs in benzene solution relative to the gas phase is reproduced quite well by a continuum solvent model, the CPCM results apparently overestimate the solvent enhancement of the spin densities on the H_{ipso} positions in water. Inclusion of explicit water molecules into the calculations reduces this enhancement and thereby tends to improve the agreement between theory and experiment.

Further analyses in terms of orbital contributions indicate that while spin polarization does to some extent influence the spin densities on the out-of-plane hydrogen or muon positions, the solvent effect derives almost exclusively from solvent-induced changes of the SOMO. It appears that the enhanced spin density at $H(Mu)_{ipso}$ is indirectly related to an increased positive charge at these out-of-plane hydrogen positions, with a concomitant negative polarization of the C_{ipso} atom by the solvent. Explicit hydrogen bonds to the π-system appear to diminish the polarization to some extent, probably mainly due to a structural effect.

Supporting information available

The dependence of hyperfine coupling in gas-phase $C_6H_7^{\bullet}$ on exchange-correlation functional (Table S1) and displays of valence molecular orbitals (Fig. S1) are available free of charge via the Internet.

Acknowledgements This project was supported by the research training group "Advanced Magnetic Resonance Type Methods in Materials Science" funded by the Deutsche Forschungsgemeinschaft (DFG) at the University of Stuttgart. Further funding came from the priority program "High-Field-EPR spectroscopy" of DFG (project KA1187/4-2).

References

1. Tolkachev VA, Molin YN, Tchkeidze II, Buben NY, Voevodsky VV (1961) Dokl Akad Nauk SSSR 141:911
2. Fischer H (1962) Kolloid-Z 180:911
3. Scheuermann R, Tucker IM, Dilger H, Staples EJ, Ford G, Fraser SJ, Beck B, Roduner E (2004) Langmuir 20:2652
4. Stolmar M, Roduner E (1998) J Am Chem Soc 120:583
5. Owenius R, Engström M, Lindgren M, Huber M (2001) J Phys Chem A 105:10967
6. Earle K, Moscicki JK, Ge M, Budil DE, Freed JH (1994) Biophys J 66:1213
7. Kurad D, Jeschke G, Marsh D (2003) Biophys J 85:1025
8. Plato M, Steinhoff H-J, Wegener Ch, Törring TT, Savitsky A, Möbius K (2002) Mol Phys 100:3711
9. Frantz S, Hübner G, Wendland O, Roduner E, Mariani C, Ottaviani MF, Batchelor SN (manuscript in preparation)
10. Webster B, Macrae RM (2000) Physica B 289–290:598
11. Roduner E (2005) In: Kohen A, Limbach HH (eds) Isotope effects in chemistry and biology. Dekker/CRC Press, New York, in press
12. Roduner E, Reid ID (1989) Israel J Chem 29:3
13. Harriman JE (1978) Theoretical foundations of electron spin resonance. Academic Press, New York
14. Barone V, Cossi M (1998) J Phys Chem A 102:1995
15. Miertus A, Scrocco E, Tomasi J (1981) Chem Phys 55:117
16. Cammi R, Tomasi J (1995) J Comp Chem 16:1449
17. Tomasi J, Persico M (1995) Chem Rev 94:2027
18. CPCM is based on the COSMO model. Klamt A, Schüürman G (1993) J Chem Soc Perkins Trans 2:799
19. Becke AD (1993) J Chem Phys 98:5648
20. Lee C, Yang W, Parr GR (1988) Phys Rev B 37:785
21. Miehlich B, Savin A, Stoll H, Preuss H (1989) Chem Phys Lett 157:200
22. Frisch MJ, Trucks GW, Schlegel HB, Scuseria GE, Robb MA, Cheeseman JR, Montgomery Jr JA, Vreven T, Kudin KN, Burant JC, Millam JM, Iyengar SS, Tomasi J, Barone V, Mennucci B, Cossi M, Scalmani G, Rega N, Petersson GA, Nakatsuji H, Hada M, Ehara M, Toyota K, Fukuda R, Hasegawa J, Ishida M, Nakajima T, Honda Y, Kitao O, Nakai H, Klene M, Li X, Knox JE, Hratchian HP, Cross JB, Bakken V, Adamo C, Jaramillo J, Gomperts R, Stratmann RE, Yazyev O, Austin AJ, Cammi R, Pomelli C, Ochterski JW, Ayala PY, Morokuma K, Voth, GA Salvador P, Dannenberg JJ, Zakrzewski VG, Dapprich S, Daniels AD, Strain MC, Farkas O, Malick DK, Rabuck AD, Raghavachari K, Foresman JB, Ortiz JV, Cui Q, Baboul AG, Clifford S, Cioslowski J, Stefanov BB, Liu G, Liashenko A, Piskorz P, Komaromi I, Martin RL, Fox DJ, Keith T, Al-Laham MA, Peng CY, Nanayakkara A, Challacombe M, Gill PMW, Johnson B, Chen W, Wong MW, Gonzalez C, Pople JA (2004) GAUSSIAN 03, Revision C.02. Gaussian, Inc, Wallingford CT, USA
23. Krishnan R, Binkley JS, Seeger R, Pople JA (1980) J Chem Phys 72:650
24. Clark T, Chandrasekhar J, Schleyer PvR (1983) 4:294

25. Barone V (1996) In: Chong DP (ed) Recent advances in density functional methods, Part I. World Scientific Publ Co, Singapore
26. Munzarová ML (2004) In: Kaupp M, Bühl M, Malkin VG (eds) Calculation of NMR and EPR parameters theory and applications. Wiley-VCH, Weinheim 2004, p 471 (and references therein)
27. Reed AE, Weinhold FJ (1985) Chem Phys 83:1736
28. Reed AE, Curtiss LA, Weinhold F (1988) Chem Rev 88:899
29. Flükiger P, Lüthi HP, Portmann S, Weber J (2000), MOLEKEL 4.0, Swiss center for scientific computing, Manno (Switzerland)
30. Portmann S, Lüthi HP (2000) Chimia 54:766
31. Courty A, Mons M, Dimicoli I, Piuzzi F, Gaigeot M-P, Brenner V, de P Pujo, Millie P (1998) J Phys Chem A 102:6590
32. Kim KS, Lee JY, Choi HS, Kim J, Jang JH (1997) Chem Phys Letters 265:497
33. Augspurger JD, Dykstra CE and Zwier TS (1992) J Phys Chem 96:7252
34. Gregory JK, Clary DC (1996) Mol Phys 88:33
35. Feller D (1999) J Phys Chem A 103:7558
36. Cheng B-M, Grover JR, Walters EA (1995) Chem Phys Letters 232:364
37. Roduner E (1988) The positive muon as a probe in free radical chemistry: potential and limitations of the μSR techniques. Lecture Notes in Chemistry. vol 49, Springer, Berlin Heidelberg, Newyork
38. Adamo C, Barone V, Subra R (2000) Theor Chem Acc 104:207
39. Experimental data for the temperature dependence of A_p show decrease with temperature by -0.0125 MHz/K in the gas phase and by ca 50% more in water or octadecane
40. Chipman DM (1992) J Phys Chem 96:3294
41. Perera SA, Salemi VM, Bartlett RJ (1997) J Chem Phys 106:4061
42. Fau S, Bartlett RJ (2003) J Phys Chem A 107:6648
43. Derzi RA, Fau S, Bartlett RJ (2003) Phys Chem A 107:6656